Volume 1 | Number 1 | Jan 2013 | Pages 1–100

Journal of
Materials Chemistry A

Materials for energy and sustainability
www.rsc.org/materialsA

ROYAL SOCIETY
OF CHEMISTRY

www.rsc.org/materialsA

Structural design of ruthenium sensitizer compatible with cobalt electrolyte for

dye-sensitized solar cell

Chia Lee, Shi-Jhang Wu, Chun-Guey Wu*

Department of Chemistry and Research Center for New Generation Photovoltaics,

National Central University, Jhong-Li, 32001, Taiwan, ROC.

E-mail address of Professor C. G. Wu: t610002@cc.ncu.edu.tw

Abstract:

Two heteroleptic ruthenium complexes, **SJW-B18** and CYC-B11H, with four alkyl groups and two alkyl groups, respectively on the terminal of their ancillary ligand were prepared. These two complexes have similar absorption profile, energy level and orbital distribution of the frontier orbitals. Therefore they are the good model compounds to explore the effect of the molecular structure of ruthenium sensitizer on their photovoltaic performance, especially when cobalt electrolyte was used in assembling the device.   When I⁻/I₃⁻ electrolyte was employed, dye-sensitized solar cell (DSSC) based on **SJW-B18** and CYC-B11H sensitizers achieved similar power conversion efficiency of 9.54% and 9.64%, respectively, due to two dyes have similar optical and electronic properties. Nevertheless when $Co^{(II)/(III)}$ electrolyte was used, **SJW-B18** sensitized device has higher efficiency (7.30%) than CYC-B11H based cell (6.65%), mainly in higher open-circuit voltage (0.829 V vs 0.784 V). Electrochemical Impedance and Intensity Modulated Photocurrent/ Photovoltage Spectroscopic data reveal that **SJW-B18** dyed TiO_2 anode has better surface protection compared to CYC-B11H adsorbed TiO_2 film. The physical insulation of the TiO_2 surface with the four alkyl groups on **SJW-B18** dye can reduce the charge recombination between the electron on TiO_2 and $Co^{(III)}$ to increase *Voc* and power conversion efficiency of the device. These results provide a new strategy for designing ruthenium sensitizers to be compatible with cobalt based electrolyte.

Key words: *dye-sensitized solar cell, ruthenium dye, cobalt electrolyte.*

1. Introduction

Looking for the affordable, renewable and no side-effect energy source is a big challenge. Dye-sensitized solar cells (DSSCs), one of the most promising photovoltaic technologies, have been developed by virtue of its colorfulness, semi-transparency, flexibility, impressive efficiency, noteworthy stability, and possible low manufacture cost.[1-3] In DSSC, upon photo excitation, the dye injects electron into the conduction band of a porous TiO_2 anode and is subsequently regenerated back to the neutral state by obtaining electron from a redox couple.[4] I_3^-/I^- redox couple is the most widely employed in DSSCs because of the regeneration of the dye by I^- is very fast and the recombination of I_3^- with the electrons in TiO_2 is extremely slow.[5] DSSC with I^-/I_3^- electrolyte has achieved remarkable photovoltaic efficiencies of over 11%[6-11] and the highest efficiency of 11.9 % is also certificated.[12] Nevertheless, I^-/I_3^- redox couple has some disadvantages, such as triiodide ion absorbs the visible light, its relatively high over-potential for dye regeneration,[13] its aggressiveness towards metal electrode, its low redox potential which limits the open-circuit voltage, and the simple structure of I^-/I_3^- prevents having molecular modification on the electrolyte to increase the *Voc* of DSSC. Therefore searching for the alternative electrolyte for DSSC becomes one of the intensive researches in the past decade.

A wide variety of redox mediators have been investigated, including halogenides,[14-15] pseudohalogenides,[16] thiols,[17-19] and metal complexes with nickel,[20] copper-,[21] iron-[22] or cobalt-[23] center. Amongst these iodine free redox couples, cobalt-based redox couple has been proven to be the most suitable one due to its weaker absorption on the visible light and less aggressive toward metallic conductors.[24,25] Conversion efficiencies (PCE) more than 10% have been reached for using cobalt-based electrolyte combining with metal free organic dye Y123 and

PEDOT cathode catalyst[26] or metal-containing porphyrin dye.[27] However, despite the extensive investigations during the last decade, DSSC based on cobalt redox mediators still exhibited lower efficiency compared to that used I^-/I_3^- couple when Ru complexes were used as sensitizers.[28-33]

Previous studies have suggested that the fast recombination of electrons in the TiO_2 with one-electron outer-sphere $Co^{(III)}$ complex[34-36] and slow diffusion of cobalt mediator as well as slow dye regeneration by $Co^{(II)}$ which limits the short circuit photocurrent density are the reasons for the poor photovoltaic performance of ruthenium based sensitizer. Fan[37,38] et al. used photoanode made from nanowire or using nanowire array anode to increase the diffusion rate of the electrolyte to improve the efficiency of DSSC based on cobalt redox couple by increasing the pore size of TiO_2 anode to facilitate the diffusion of Co-based electrolyte. Hagfeldt[39] *et al.* suggested that by introducing a long-chain alkyoxy groups in dye molecule can retard the unwanted charge recombination process to improve the device's efficiency. Recently Frey[40] *et al.* also demonstrated that cyclometalated $Ru^{(II)}$ sensitizer with steric cyclometalating ring (and two alkoxyl substitutes) also compatible with cobalt redox couple (8.6% for cobalt electrolyte *vs* 8.7% based on Iodine electrolyte). They used transient absorption decay and charge extraction measurements to show that the kinetics of charge recombination and dye regeneration are similar for two types of electrolytes. Detailed studies show that the recent breakthrough in efficiency of ruthenium sensitizer with Co-based redox electrolytes are due to a reduction of interfacial recombination through the increase of the steric bulkiness of a selected dye, enhancing the charge collection efficiency. Therefore the high efficiency of cobalt based device is directly correlated to the good TiO_2 surface protection, preventing the recombination between the electrons in TiO_2 and $Co^{(III)}$ species in the electrolyte.[24,25]

In this work we reported the synthesis and photovoltaic performance of a new Ru

sensitizer **SJW-B18** (its molecular structure is presented in Figure 1), specially designed for using in DSSC with cobalt electrolyte. **SJW-B18** has four alkyl groups on the terminal of the ancillary ligand, which can form a protection layer when adsorbed on TiO$_2$ to avoid the charge recombination. To prove the surface of dye adsorbed TiO$_2$ film can be protected with the alkyl chains on the sensitizer, another ruthenium dye, CYC-B11H (the structure is also displayed in Figure 1, its ammonia counterpart was reported before[9]), was also prepared for the comparison. CYC-B11H and **SJW-B18** dyes have similar optical and electronic properties and the only difference in structure is the number of terminal alkyl chains. Therefore when Co$^{(II)/(III)}$ electrolyte was used in the device, the variation in the photovoltaic performance between these two dyes can provide some information for designing ruthenium dye compatible with cobalt electrolyte.

2. Experimental

2.1 Materials and characterization: All reagents were obtained from the commercial resources and used as received unless specified. Solvents were dried over sodium or CaH$_2$ before use. The structure of the dyes was identified with ^{1}H-NMR spectrum, FAB-MS and elemental analysis. ^{1}H-NMR spectra were recorded with a DRX-500 NMR spectrometer in CDCl$_3$ or DMSO-d$_6$. FAB-MS spectra were obtained using a JMS-700 HRMS system. Elemental analyses were carried out with a Heraeus CHN-O-S Rapid-F002 analysis system. UV/Vis spectra were measured using a Cary 300 Bio spectrometer. Electrochemical study of the dye dissolved in DMF was performed in a single-compartment, three-electrode cell with a Pt wire counter electrode. The reference electrode was Ag/Ag$^+$ and the supporting electrolytes were 0.1 M tetrabutylammonium hexafluorophosphate (TBAPF$_6$) in dimethylformamide (DMF). The square-wave voltammograms (potential step increment: 10 mV; frequency:

25 Hz) were recorded using a potentiostat/galvanostat (PGSTAT 30, Autolab, Eco-Chemie, the Netherlands) and ferrocene was used as a calibration external standard. The DFT calculation based on a Gaussian 09 program,[41] adopting the B3LYP/DGDZVP function and basis set,[42] was used in combination with the C-PCM,[43] applied to account for the solvation effects, to optimize the geometry and calculate the frontier orbital distribution of the dye molecule in DMF.

Synthesis of SJW-B18 (Ru[(dcbpy)(Ligand-18)(NCS)$_2$]) and CYC-B11H: Ligand-18 for **SJW-B18** was prepared by the alkylation and Stille coupling reactions. The detailed synthetic procedures can be found in the electronic supporting information (ESI). **SJW-B18** was synthesized using an one-pot method similar to the reaction protocol we had reported previously:[44] 0.22 g (0.36 mmol) [RuCl$_2$(p-cymene)]$_2$, 0.50 g (0.71 mmol) Ligand-18, 0.10 g (0.41 mmol) dcbpy and excess (8.0 mmol) NH$_4$NCS were used sequentially in the reaction. The crude product was dissolved in a mixture of methanol and aqueous solution of tetra-butyl ammonium hydroxide (TBAOH, 40 wt% in H$_2$O) and then purified on a Sephadex LH-20 column using methanol as an eluent. The main band was collected and the pH value of the collected solution was adjusted to *ca.* 3 by adding 0.1 M HNO$_{3(aq)}$. The collected precipitate was washed with water and dried under vacuum. After further purification, 0.150 g (0.12 mmol, 18.1% yield) of deep purple **SJW-B18** was obtained. ^{1}H-NMR (500 MHz, δ/ppm in DMSO-d$_6$, *J* Hz): 9.45 (d, *J* = 5.61 Hz, 1H); 9.16 (d, *J* = 5.96 Hz, 1H); 9.11 (s, 1H); 9.07 (s, 1H); 8.96 (s, 1H); 8.92 (s, 1H); 8.33 (d, *J* = 5.66 Hz, 1H); 8.24 (d, *J* = 3.68 Hz, 1H); 8.18 (d, *J* = 6.05 Hz, 1H); 8.03 (d, *J* = 3.80 Hz, 1H); 7.95 (d, *J* = 5.81 Hz, 1H); 7.65(d, *J* = 6.05 Hz, 1H); 7.51 (d, *J* = 3.6 Hz, 1H); 7.42 (d, *J* = 6.09 Hz, 1H); 7.39 (d, *J* = 3.75 Hz, 1H); 7.35 (d, *J* = 6.15 Hz, 1H); 7.30 (s, 1H); 7.20 (s, 1H); 2.73 (m, 8H); 1.57 (m, 8H); 1.32 (m, 8H); 0.91 (m, 12H). MS calcd: *m/z* 1170.3 ([M]$^+$). HRFAB-MS found: *m/z* 1170.1731 (m) ([M]$^+$); 1112.3 (s) ([M-NCS]$^+$). Elemental

analysis: calcd. for $C_{56}H_{56}N_6O_4RuS_6 \cdot 1.5H_2O$: C, 56.06; H, 4.92; N, 7.00; S, 16.02 %. Found: C, 55.89; H, 5.16; N, 6.85; S, 15.60 %.   CYC-B11H was prepared and identified very similar to our previous report.[8]   The detailed preparation steps can be found in ESI.

DSSC Device fabrication and characterization: 12 μm (or 4 μm) thick transparent layer (20 nm in diameter) and 4 μm of scattering layer of anatase TiO_2 (400 nm in diameter, prepared in our lab.) were deposited sequentially on fluorine-doped tin oxide (FTO) conducting glass to make the photoanode. Detailed methods for TiO_2 film preparation and device fabrication can be found in our earlier report.[45] TiO_2 film was immersed into a 300 μM solution of **SJW-B18** or CYC-B11H containing 20 ~ 30 mmol CDCA as a co-adsorbent in a mixture of acetonitrile and *tert*-butyl alcohol (volume ratio 1:1) at room temperature for 3 (for thin TiO_2 film) and 12 h (for thick TiO_2 film). Two types of electrolytes with different active ingredients (listed below the tables containing the photovoltaic data) were used for the device fabrication. The photocurrent-voltage characteristics were obtained by applying an external voltage bias to the devices exposing to an irradiance of AM 1.5 Sun light (100 mW cm^{-2}) given by a 450 W xenon light source (Yamashida Co., Japan), while measuring the generated photocurrent using Keithley model 2400 digital source meter (Keithley, USA). The illuminated active area was 0.25 cm^2 square using a metal mask.

The dye loading was measured by desorbing the dye molecules from the practical TiO_2 anode with a solution of 0.1 g/mL tetra-butyl ammonium hydroxide (TBAOH)/ dimethylformamide (DMF). A calibration curve of the dye in TBAOH/DMF solution was made and the number of dye molecules adsorbed on TiO_2 anode was determined by the absorption spectrum using the calibration curve.

Transient absorption spectroscopy (TAS): TAS measurements were performed in Proteus Ultrafast System with the light pass designed by our lab.   A laser light was

used to excite the dye molecules in DSSC device and a white light was passed through the device to measure the absorption of the excited dye molecules. The decay of the absorption intensity at 820 nm was used to study the regeneration kinetics of the excited dye. The rate constants (or decay time) were extracted by fitting the data using a Surface Xplorer software to obtain the rates for the regeneration of the dye molecules by I^- in the redox couple and electron in TiO_2.[46]

Electrochemical impedance spectroscopy (EIS): EIS measurement was carried out with an Autolab PG30stat (Eco-Chemie, the Netherlands) in 50 mV voltage steps and with a sinusoidal potential perturbation of 10 mV in the dark. The applied voltage is close to the *Voc* of the measured device and the potential perturbation was applied over a frequency range of 0.1 Hz to 1.0 MHz. The resulting impedance spectra were fitted according to the transmission line model proposed by Bisquert[47] *et al*. with the Z-View software from Scribner.

Intensity Modulated Photocurrent/Photovoltage Spectroscopy (IMPS/ IMVS). IMPS/IMVS was used to study the charge transport and back recombination reaction occurred in DSSC. The experimental setup for the measurement is similar to that described in literature.[48] IMPS/IMVS response was recorded with a Zenniumm CIMPS-1 potenstat (Zahner Co.) installed with a light intensity modulated function. The light source used is Xpot-26341 and light intensity corresponds to 1/20 (5 mW/cm^2) to 1/3 (33.3 mW/cm^2) Sun was used. The potential perturbation was applied over a frequency range of 0.1 Hz to 10 kHz with amplitude of 10 mV. The electron life time (τ_n or τ_d), electron diffusion coefficient (D_n) and electron diffusion length (L_n) were calculated according to the equations of $\tau_n = 2\pi f_{min} (IMVS))^{-1}$ (or $\tau_d = (2\pi f_{min} (IMPS))^{-1}$, $D_n = d^2/4\tau_n$ and $Ln = (D_n\tau_n)^{1/2}$, f_{min}: the minimum frequency of the IMPS response, d: thickness of TiO_2), proposed by Krüger[43] *et al.*

8

3. Results and Discussion

3.1 Synthesis of ruthenium dyes and their optical property.

The ancillary ligand (Ligand 18) of **SJW-B18** was synthesized according to Scheme 1. The detailed synthetic procedures and structure identification of each intermediate and final product can be found in ESI. **SJW-B18** was synthesized using an one-pot method (described in the Experimental Section) similar to the reaction protocol we had reported previously.[44] CYC-B11H is a proton form of CYC-B11 we reported before.[9] The detail steps for converting the ammonia form (CYC-B11) to the proton form (CYC-B11H) was also described in ESI. The electronic absorption spectra of **SJW-B18** and CYC-B11H measured in DMF and immobilized on the transparent TiO$_2$ film (thickness is *ca.* 3 μm) are displayed in Figure 2. **SJW-B18** dissolved in DMF displays two intense absorption bands centred at 395 nm and 558 nm. The high energy band is assigned to the overlap of the ancillary ligand intra-ligand π-π* transitions and one of the MLCT (metal-to-ligand charge transfer) bands. The low energy band at 558 nm with a molar absorption coefficient (ε) of 2.16×10^4 M^{-1} cm^{-1} is attributed to another MLCT transition which determines the *Jsc* of the corresponding device. CYC-B11H in DMF has MLCT band centred at 557 nm with a ε of 2.40×10^4 M^{-1} cm^{-1} which is higher than that of **SJW-B18**, probably due to the latter has lower molecular weight. When **SJW-B18** is anchored onto the surface of a transparent TiO$_2$ film, a slight blue-shift (*ca.* 6 nm) of the MLCT band is observed along with a slight change in the absorption profile, which is induced by the effect of de-protonation in the dye self-assembly process and maybe the conformation of dye molecules also changed after adsorbed on TiO$_2$. Similar phenomenon was observed when CYC-B11H adsorbed on TiO$_2$ film. Comparing the absorption spectra of both dyes adsorbed TiO$_2$ thin films, the absorption profiles are similar except the absorption intensity of the MLCT band for **SJW-B18** dyed thin film is slightly weaker (due to

lower dye loading or smaller absorption coefficient).

3.2 Energy level and isodensity surface plots of the frontier orbitals for SJW-B1 and CYC-B11H dyes.

To investigate the driving force for the electron injection from photo-excited dye into the conduction band of TiO_2 and the regeneration of oxidized dye by the redox couple, square-wave voltammetry of **SJW-B1** and CYC-B11H was performed (the data was displayed in Figure S1, ESI). The energy levels of the ground and excited states for **SJW-B18** and CYC-B11H determined by combining the oxidation potential and the absorption threshold (in DMF) are displayed in Table 1**.** The ground state potential of **SJW-B18** dissolved in DMF is 0.95 V *versus* NHE (-5.45 eV *versus* vacuum), which is close to that (0.96 V *versus* NHE) of CYC-B11H and more positive than the redox potential of the iodide/triiodide or $Co(bipy)_3^{II/III}$ redox couple used in this study, both oxidized dyes can be reduced effectively by the electrolyte. The excited state oxidation potential ($E_{S+/S*}$) of **SJW-B18** (*ca.* - 0.60 V *vs*. NHE) and CYC-B11H (*ca.* - 0.61 V *vs*. NHE) are also almost the same (within the experimental error), both dyes have a sufficient driving force for the electron injection form excited dye into TiO_2 conduction band (EC = *ca.*-0.5 V vs. NHE). These data indicate that the number and length of the alkyl chains at the end of ancillary ligands will not significantly affect the electronic state of the heteroleptic ruthenium sensitizer.

The graphical representation of the computed frontier orbitals for **SJW-B18** and CYC-B11H are shown in Figure 3. The HOMOs (highest occupied molecular orbitals) of both dyes contribute primarily from Ru-NCS mixed orbitals and the LUMOs (lowest unoccupied molecular orbitals) are localized on 4,4'-dicarboxyvinyl-2,2'-bipyridine anchoring ligands. Not only the participation and energy level of the frontier orbitals for two dyes but also the energy of MLCT band (see the following

paragraph) are similar between **SJW-B18** and CYC-B11H. Since the optical and electronic properties of two sensitizers are similar, the photovoltaic performance of the corresponding devices was affected only by the structure of the dye molecules and the absorptions (dye loading times absorption coefficient) of dyes adsorbed on TiO_2 anodes. **SJW-B18** and CYC-B11H dyes are therefore a good couple to study the effect of the molecular structure of ruthenium sensitizer on the surface protection of dye adsorbed TiO_2, therefore the photovoltaic performance of DSSC devices when cobalt complexes are used as a redox couple.

3.3 Photovoltaic performance of ruthenium sensitizers.

To demonstrate that both **SJW-B18** and CYC-B11H are excellent sensitizers for DSSC, devices based on I^-/I_3^- electrolyte were studied first. The characteristic *I-V* and *IPCE* curves of the devices (device A and B) sensitized with **SJW-B18** and CYC-B11H, measured under the illumination of AM 1.5G simulated sunlight (100 mWcm^{-2}), are displayed in Figure 4. The detailed photovoltaic parameters and dye loading are also collected in Table 1. The power conversion efficiency (9.54%) of **SJW-B18** sensitized device (device A) is slightly lower than that (9.64%) for the device sensitized by CYC-B11H (device B), mainly in smaller Jsc, probably due to the latter has more dyes with higher absorption coefficient adsorbed on TiO_2 anode. The corresponding incident photon-to-current conversion efficiency (IPCE) spectra of the device A and B presented in Figure 4b show a strong spectral response in the range from 450 nm to 650 nm, having a maximum efficiency of 82% (at 543 nm), and 81% (at 550 nm) for the devices based on **SJW-B18** and CYC-B11, respectively. These results substantiate that the electron injection from photo-excited sensitizers to the conduction band of TiO_2 occurs efficiently even though the driving potential for electron injection is less than 0.3 eV.

Transient absorption spectra (TAS, see Figure S2, ESI) of the device A and B were taken to explore the reduction dynamic/path of the oxidized dye. The dye regeneration life times ($\tau 1$ and $\tau 2$ corresponding to the reduction of oxidized dye molecules by I^- in electrolyte and by the electrons in TiO_2, respectively[49-50]) and the amplitudes ratios for $\tau 1$ and $\tau 2$ are listed in Table 2. TAS data show that $\tau 1$ and $\tau 2$ for the device A and device B are not the same but $\tau 1/\tau 2$ amplitude ratios are similar. This result suggests that the ratio for reducing the oxidized dye by iodide in electrolyte and by electron on TiO_2 is similar for device A and B. Therefore higher *Jsc* for the device B compared to the device A is mainly due to more CYC-B11H dye with higher absorption coefficient was adsorbed on TiO_2 anode.

The characteristic *J-V* and *IPCE* curves of **SJW-B18** and CYC-B11 sensitized devices (device C and D) based on $[Co^{II/III}(bipy)_3]^{2/3+}$ (tris(4,4'-bipyridine)-cobalt-(II/III), E^0 = +0.62 V *vs* NHE) electrolyte are shown in Figure 5 and the photovoltaic parameters are listed in Table 3. The thickness of TiO_2 photoanode used in device C and D are the same as those applied in I^-/I_3^- based devices. As expected, using thick TiO_2 anode, the efficiency (especially *Jsc*) of the devices used $[Co^{II/III}(Bipy)_3]^{2/3+}$ electrolyte are much lower than those for the devices based on I^-/I_3^- redox couple, due to the low mass transport rate related to the bulky size of $Co^{(II/III)}$ complexes and the facile charge recommendation due to the positive nature of cobalt electrolyte.[24] The injected electron will recombined with Co-electrolyte before diffusing to anode and $Co^{(III)}$ diffuses slowly to cathode to accept the electron and finish the photo-to electricity conversion process. IPCE curves for both devices a and B also show that the efficiency is very low (<60%) at the whole measured wavelength. Nevertheless, **SJW-B18** sensitized devices has higher *Voc* compared to CYC-B11H based device, which may due to TiO_2 anode in device C has better surface protection. To explore the surface coverage of TiO_2, electrochemical impedance measurements (see Figure S3,

ESI) of the devices C and D were performed under dark. The charge transfer resistance (Rct) at dyed TiO_2/electrolyte interface estimated from the middle frequency semicircle was also displayed in Table 3. Device C has higher Rct value suggested that **SJW-B18** dyed TiO_2 has better surface protection. Furthermore, the IPCE curves for the devices based on $Co^{(II/III)}$ electrolyte with thick TiO_2 anode are very consistent with the absorption spectra of dye adsorbed on TiO_2 thin films (see Figure 2a). These data suggested that the excited dye molecules can inject electrons into TiO_2 efficiently after absorbing photons. Nevertheless only small ratio of electrons on TiO_2 can diffuse to the external circuit to produce electricity. Most injected electrons on TiO_2 (especially those far away from the anode) recombined with $Co^{(III)}$ species in the electrolyte, due to the facile reduction of $Co^{(III)}$ species and the slow diffusion rate of the bulky cobalt complex.

Optimizing the device by changing the thickness of TiO_2 anode and dye loading time, the *J-V* and IPCE curves of the optimized devices (device E and F) are shown in Figure 6. The photovoltaic performance and the dye loading are also listed in Table 3. When the thickness of TiO_2 was reduced from 12+4 μm to 4+4 μm and the dye loading time decreases from 12 h to 3 h, the power conversion efficiency of **SJW-B18** sensitized device increased from 3.84% to 7.30%. The efficiency of CYC-B11H sensitized device also increases from 3.89% to 6.65%. This is a general phenomenon when cobalt redox couple was used as an electrolyte in DSSC: the highest efficiency occurs at thinner TiO_2 anode compared to the device used I^-/I_3^- electrolyte. As mentioned in the previously paragraphs, the characteristics of cobalt electrolyte are facile charge recombination with the electrons in TiO_2 (or even in FTO[51]) due to its positively charge nature and slow diffusion rate (an order of magnitude slower than I_3^- in bulk solution) attribute to the high mass of the cobalt complex, higher viscosity of the electrolyte and electrostatic surface interaction between the cobalt complex and

TiO$_2$ film. When the thickness of TiO$_2$ film was used, more dye can adsorb and inject more electrons to TiO$_2$ anode. However, the injected electrons on TiO$_2$ far away from FTO (or external circuit) will recombine with cobalt electrolyte without contributing Jsc. On the other hand, TiO2 is a high band-gap semiconductor with low conductivity. Thicker film has higher resistance, therefore lower FF, resulting in lower efficiency. As a result, the optimal TiO2 thickness for the device using cobalt electrolyte is thinner compared to the device based on iodine electrolyte. The efficiency of **SJW-B18** and CYC-B11H sensitized devices is almost the same when I$^-$/I$_3^-$ redox couple was used. On the other hand, when cobalt complex was used as an electrolyte, the device sensitized by **SJW-B18** has better photovoltaic performance, mainly in higher *Voc* and *FF*, compared to that based on CYC-B11H.

SJW-B18 and CYC-B11H have the similar structure (see Figure 1), orbital distribution and energy level of the frontier orbitals (HOMO and LUMO, Figure 3 and Table 1). The driving force for injecting electron from the excited dye to TiO$_2$ anode and reducing the oxidized dye molecules by electrolyte is nearly the same. Transient absorption data (Table 2) of the devices based on I$^-$/I$_3^-$ electrolyte discussed in the previous paragraph also revealed that the ratio of the effective reduction (by I$^-$ in the electrolyte and by electron in TiO$_2$) of the oxidized dye molecules did not have a significant difference for **SJW-B18** and CYC-B11H sensitized devices. The absorption profile of **SJW-B18** adsorbed TiO$_2$ thin film is also comparable to that for CYC-B11H dyed film (see Figure 2). Furthermore the absorption (dye loading times absorption coefficient of dye) for **SJW-B18** on TiO$_2$ anode even lower than CYC-B11H sensitized TiO$_2$ (Table 3). Therefore the better photovoltaic performance of **SJW-B18** based device may be mainly attributed to the less charge recombination between the electrons on TiO$_2$ anode and cobalt electrolyte. Charge recombination in DSSC was known to be dependent of the surface protection of the dye adsorbed TiO$_2$

anode.[46,52]   **SJW-B18** with four alkyl groups on the terminal of the ancillary ligand

can form better TiO_2 surface protection compared to CYC-B11H which has only two

alkyl groups on the ancillary ligand. Reducing the back charge recombination in

accounting for the improving in *V*oc and photovoltaic performance of the device

based on $Co^{(II)/(III)}$ redox couple evidently stem from the increase in the number of

alkyl group on the ancillary ligands of ruthenium sensitizer.

3.4 Study the surface protection of the dye adsorbed TiO_2 anode by EIS and

IMPS/IMVS technique.

The evidence of the surface coverage for dyed TiO_2 anodes in the device E and F

comes from the electrochemical impedance data (see Figure S3b, ESI) taken under

dark. The simulated charge transfer resistance (Rct) are also listed in Table 3. Rct for

SJW-B18 based device is larger than that for the device sensitized with CYC-B11H,

suggesting that the interfacial back charge recombination of the electron on TiO_2 with

Co^{III} species is retarded when the sensitizer has more terminal alkyl groups, which

may account for the higher *Voc* and η for **SJW-B18** sensitized device.   In order to

obtain more information regarding to the surface protection of dyed TiO_2 anode, the

intensity modulated photocurrent/photovoltage spectra (IMPS/IMVS) for both

SJW-B18 and CYC-B11H sensitized devices (device C, D, E and F) were taken.

IMPS data can provide the information regarding to the diffusion of electron in TiO_2

and the life time of electron in TiO_2 can be derived from IMVS results.[53] For thick

TiO_2 anodes, the effective electron diffusion coefficient (D_n, see Figure 7a) for

SJW-B18 sensitized device (device C) is smaller than that for CYC-B11H based

device (device D), due to the former has less dye with smaller absorption coefficient

adsorbed on TiO_2 (see Table 3).   Nevertheless, Figure 7b clearly illustrated that the

life time (τ_n, obtained from the IMVS data) of the electrons on TiO_2 is longer for

SJW-B18 sensitized device (device C) compared to device D. Longer electron life time indicated less charge recombination occurs or more electrons on TiO_2 (the latter is not the truth since the absorption of **SJW-B18** dyed TiO_2 is weaker than that for CYC-B11H adsorbed TiO_2). Less charge recombination suggested that **SJW-B18** dyed TiO_2 anode has better surface protection, consistent with EIS data.

When thin (4+4 μm) TiO_2 anode was used, IMPS data (Figure 8a) showed that D_n for **SJW-B18** sensitized device (device E) is only slightly smaller than that for CYC-B11H based device (device F) and the D_n values for both device E and F are smaller than those for the device C and D (with thick TiO_2 anode). D_n value depends on the quality of TiO_2 and the number of injected electrons. Device with thinner TiO_2 anode was loaded with less dye molecules therefore has smaller D_n value. The absorption of **SJW-B18** dyed anode is only slightly lower than that of CYC-B11H dyed TiO_2 (see Table 3) therefore D_n values for the device C and D are also very close. Nevertheless, *Jsc* for the device E and F with less dye on TiO_2 film (thin anode) is higher than that for the device C and D with more dye on TiO_2 film (thick anode, see Table 3). The results suggest that most injected electrons on thick TiO_2 anode recombined with the cobalt electrolyte before diffusing to FTO electrode. The τ_n values for the device E and F (used thin TiO_2 anodes) are longer than those for the device C and D based on thick TiO_2 films. That is why *Jsc* for the devices with thin anode is higher than those for the devices with thick TiO_2 film; even more electrons were injected in thicker TiO_2 anode upon photo exciting of the dye molecules. τ_n value for the device E is longer than that for the device F under all light intensity, indicated that device E has less charge recombination, which is due to the better surface protection of TiO_2 anode. IMPS/IMVS data undeniably reveal the importance of TiO_2 surface protection when high current density of the cobalt based devices was expected and the protection of sensitized TiO_2 anode can be improved by simply

adding more alkyl chains to the sensitizer.

4. Conclusions

In summary, we report the synthesis and photovoltaic performance of two new ruthenium sensitizers, **SJW-B18** and CYC-B11H, specially designed to study the compatibility between ruthenium dye and cobalt electrolyte. These two ruthenium sensitizers have similar electronic and optical properties but **SJW-B18** dye with four butyl chains in the terminal of the ancillary ligand and there are only two octyl chains in the ancillary ligand of CYC-B11H dye. The conversion efficiencies based on I^-/I_3^- electrolyte for **SJW-B18** and CYC-B11H sensitized devices (9.54% and 964%, respectively) are very close, consistent with the two complexes have similar electronic and optical properties. However when $Co^{(II)/(III)}$ redox shuttle was used as an electrolyte, the device sensitized with **SJW-B18** has higher *Voc* and η compared to CYC-B11H based device. The better photovoltaic performance of **SJW-B18** sensitized device is mainly due to **SJW-B18** dyed TiO_2 anode has better surface protection by four alkyl chains in the terminal of the ancillary ligand as evidenced by EIS and IMPS/IMVS data. The results provide a new strategy for developing high open-circuit voltage (without sacrificing *Jsc*) DSSCs through structure design of ruthenium sensitizer.

Acknowledgements

References:

1 B. O'Regan and M. Grätzel, *Nature,* 1991, 353, 737**.**

2 M. Grätzel, *Acc. Chem. Res.,* 2009, 42, 1788.

3 A. Hagfeldt, G. Boschloo, L. Sun, L. Kloo and H. Pettersson, *Chem. Rev.,* 2010, 110*,* 6595.

4 A. Hagfeldt and M. Grätzel, *Acc. Chem. Res.,* 2000, 33, 269.

5 B. A. Gregg, F. Pichot, S. Ferrere and C. R. Fields, *J. Phys. Chem. B,* 2001, 105, 1422.

6 M. K. Nazeeruddin, F. De Angelis, S. Fantacci, A. Selloni, G. Viscardi, P. Liska, S. Ito, B. Takeru and M. Grätzel, *J. Am. Chem. Soc.,* 2005, 127, 16835.

7 F. Gao, Y. Wang, D. Shi, J. Zhang, M. Wang, X. Jing, R. Humphry-Baker, P. Wang, S. M. Zakeeruddin and M. Grätzel, *J. Am. Chem. Soc.,* 2008, 130, 10720.

8 Y. Cao, Y. Bai, Q. Yu, Y. Cheng, S. Liu, D. Shi, F. Gao and P. Wang, *J. Phys. Chem. C,* 2009, 113, 6290.

9 C. Y. Chen, M. Wang, J. Y. Li, N. Pootrakulchote, L. Alibabaei, C. H. Ngoc-le, J. D. Decoppet, J. H. Tsai, C. Grätzel, C. G. Wu, S. M. Zakeeruddin and M. Grätzel, *ACS Nano,* 2009, 3, 3103.

10 Q. Yu, Y. Wang, Z. Yi, N. Zu, J. Zhang, M. Zhang and P. Wang, *ACS Nano,* 2010, 4, 6032.

11 A. Yella, H. W. Lee, H. N. Tsao, C. Yi, A. K. Chandiran, M. K. Nazeeruddin, E. W. G. Diau, C. Y. Yeh, S. M. Zakeeruddin and M. Grätzel, *Science,* 2011, 334, 629.

12 http://www.nrel.gov/ncpv/images/efficiency_chart.jpg.

13 G. Boschloo and A. Hagfeldt, *Acc. Chem. Res.,* 2009, 42, 1819.

14 Z.-S. Wang, K. Sayama and H. Sugihara, *J. Phys. Chem. B,* 2005, 109, 22449.

15 C. Teng, X. C. Yang, C. Z. Yuan, C. Y. Li, R. K. Chen, H. N. Tian, S. F. Li, A.

Hagfeldt and L. C. Sun, *Org. Lett.,* 2009, 11, 5542.

16 G. Oskam, B. V. Bergeron, G. J. Meyer and P. C. Searson, *J. Phys. Chem. B,* 2001, 105, 6867.

17 M. K. Wang, N. Chamberland, L. Breau, J. E. Moser, R. Humphry-Baker, B. Marsan, S. M. Zakeeruddin and M. Grätzel, *Nat. Chem.,* 2010, 2, 385.

18 J. Burschka, V. Brault, S. Ahmad, L. Breau, M. K. Nazeeruddin, B. Marsan, S. M. Zakeeruddin and M. Grätzel, *Energy Environ. Sci.*, 2012, 5, 6089.

19 P. Wang, S. M. Zakeeruddin, J. E. Moser, R. Humphry-Baker and M. Grätzel, *J. Am. Chem. Soc.,* 2004, 126, 7164.

20 A. M. Spokoyny, T. C. Li, O. K. Farha, C. W. Machan, C. She, C. L. Stern, T. J. Marks, J. T. Hupp and C. A. Mirkin, *Angew. Chem., Int. Ed.,* 2010, 49, 5339.

21 S. Hattori, Y. Wada, S. Yanagida and S. Fukuzumi, *J. Am. Chem. Soc.,* 2005, 127, 9648.

22 T. Daeneke, T.-H. Kwon, A. B. Holmes, N. W. Duffy, U. Bach and L. Spiccia, *Nat. Chem.,* 2011, 3, 213.

23 H. Nusbaumer, S M. Zakeeruddin, J-E. Moser and M. Grätzel, *Chem. Eur. J.,* 2003, 9, 3756.

24 M. Wang, C. Grätzel, S. M. Zakeeruddin and M. Grätzel, *Energy Environ. Sci.*, 2012, 5, 9394.

25 J. Cong, X. Yang, L. Kloob and L. Sun, *Energy Environ. Sci.*, 2012, 5, 9180.

26 H. N. Tsao, J. Burschka, C. Yi, F. Kessler, M. K. Nazeeruddin and M. Grätzel, *Energy Environ. Sci.,* 2011, 4, 4921.

27 A. Yella, H. W. Lee, H. N. Tsao, C. Yi, A. K. Chandiran, M. K. Nazeeruddin, E. W. G. Diau, C. Y. Yeh, S. M. Zakeeruddin and M. Grätzel, *Science,* 2011, 334, 629.

28 B. M. Klahr and T. W. Hamann, *J. Phys. Chem. C,* 2009, 113, 14040.

29 S. Cazzanti, S. Caramori, R. Argazzi, C. M. Elliott and C. A. Bignozzi, *J. Am. Chem. Soc.,* 2006, 128, 9996.

30 H. Nusbaumer, S. M. Zakeeruddin, J.-E. Moser and M. Grätzel, *Chem. Eur. J.*, 2003, 9, 3756.

31 H. Nusbaumer, J.-E. Moser, S. M. Zakeeruddin, M. K. Nazeeruddin and M. Grätzel, *J. Phys. Chem. B,* 2001, 105, 10461.

32 Y. Liu, J. R. Jennings, Y. Huang, Q.Wang, S. M. Zakeeruddin and M. Grätzel, *J. Phys. Chem. C,* 2011, 115, 18847.

33 S. M. Zakeeruddin, M. K. Nazeeruddin, R. Humphry-Baker, P. Pchy, P. Quagliotto, C. Barolo, G. Viscardi and M. Grätzel, *Langmuir*, 2002, 18, 952.

34 B. A. Gregg, F. Pichot, S. Ferrere and C. L. Fields, *J. Phys. Chem. B,* 2001, 105, 1422.

35 B. M. Klahr and T. W. Hamann, *J. Phys. Chem. C,* 2009, 113, 14040.

36 S. Nakade, Y. Makimoto, W. Kubo, T. Kitamura, Y. Wada and S. Yanagida, *J. Phys. Chem. B,* 2005, 109, 3488.

37 J. Fan, Y. Hao, A. Cabot, E. M. Johansson, G. Boschloo and A. Hagfeldt. *ACS Appl. Mater. Interfaces* 2013, 5, 1902..

38 J. Fan, C. Fabrega, R. R. Zamani, Y. Hao, A. Parra, T. Andreu, J. Arbiol, G. Boschloo, A. Hagfeldt, Anders, M. Ramon, C. Joan, J. R. Morante and A. Cabot *ACS Appl. Mater. Interfaces* 2013, 5, 9872.

39 S. M. Feldt, E. A. Gibson, E. Gabrielsson, L. Sun, G. Boschloo and A. Hagfeldt, *J. Am. Chem. Soc.,* 2010, 132, 16714.

40 L. E. Polander, A. Yella, B. F. E. Curchod, N. A. Astani, J. Teuscher, R. Scopelliti,

P. Gao, S. Mathew, J.-E. Moser, I. Tavernelli, U. Rothlisberger, M. Grätzel, Md. K. Nazeeruddin and J. Frey, *Angew. Chem. Int. Ed.,* 2013, 52, 8731.

41 A. Reynal, A. Forneli, E. Martinez-Ferrero, A. Sánchez-Díaz, A. Vidal-Ferran, B. O'Regan and E. Palomares, *J. Am. Chem. Soc.,* 2008, 13*0*, 13558.

42 B. O'Regan, K. Walley, M. Juozapavicius, A. Anderson, F. Matar, T. Ghaddar, S. M. Zakeeruddin, C. Klein and J. R. Durrant, *J. Am. Chem. Soc.,* 2009, 131, 3541.

43 J. Krüger, R. Plass, M. Grätzel, P. J. Cameron and L. M. Peter, *J. Phys. Chem. B*, 2003, 107, 7536.

44 C. Y. Chen, S. J. Wu, C. G. Wu, J. G. Chen and K. C. Ho, *Angew. Chem.Int. Ed.,* 2006, 118, 5954.

45 J.-Y. Li, C.-Y. Chen, C.-P. Lee, S.-C. Chen, T.-H. Lin, H.-H. Tsai, K.-C. Ho and C.-G. Wu, *Org. Lett.,* 2010, 12, 5454.

46 A. J. Mozer, D. K. Panda, S. Gambhir, B. Winther-Jensen and G. G. Wallace, *J. Am. Chem. Soc.,* 2010, 132, 9543.

47 F. Fabregat-Santiago, G. Garcia-Belmonte, J. Bisquert, A. Zaban and P. Salvador, *J Phys. Chem. B,* 2002, 106, 334.

48 L. M. Peter and K. G. U. Wijayamtha, *Electrochim Acta,* 2000, 45, 4543.

49 M. Cossi, N. Rega, G. Scalmani and V. Barone, *J. Comput. Chem.,* 2003, 24, 669.

50 C.-Y. Chen, M. Wang, J.-Y. Li, N.Pootrakulchote, L. Alibabaei, C. Ngoc-le, J.-D. Decoppet, J.-H. Tsai, C. Grätzel, C.-G. Wu, S. M. Zakeeruddin and M. Grätzel, *ACS Nano,* 2009, 3, 3103

51 H. Nusbaumer, S. Zakeeruddin, J. Moser and M. Grätzel, *Chem. Eur. J.*, 2003, 9, 3756.

52 A. Hagfeldt and M. Grätzel, *Chem. Rev.,* 1995, 95, 49.

53 A. Y. Anderson, P. R. F. Bames, J. R. Durrant and B. C. O'Regan, *J. Phys. Chem. C,* 2011, 115, 2439.

Figure captions:

Scheme 1: Procedure for preparing Ligand 18.

Figure 1: Molecular structure of **SJW-B18** and CYC-B11H.

Figure 2: Electronic absorption spectra of **SJW-B18** and CYC-B11H (a) dissolved in DMF and (b) anchored on transparent TiO_2 films (thickness of *ca.* 4 μm).

Figure 3: Isodensity surface plots of the frontier orbitals (LUMO and HOMO) for **SJW-B18** and CYC-B11H. (isodensity value = 0.03).

Figure 4: Photocurrent density-voltage (*I-V*) and IPCE curves of the devices (device A, B) sensitized with **SJW-B18** and CYC-B11H, respectively measured under AM 1.5G simulated sunlight illumination (100 mW /cm^2).

Figure 5: Photocurrent density-voltage (*I-V*) and IPCE curves for device C and D sensitized with **SJW-B18** and CYC-B11H, respectively measured under AM 1.5G simulated sunlight illumination (100 mW /cm^2). (Thickness of TiO_2 film: 12+4 μm).

Figure 6: Photocurrent density-voltage (*I-V*) and IPCE curves for device E and F sensitized with **SJW-B18** and CYC-B11H, respectively measured under AM 1.5G simulated sunlight illumination (100 mW /cm^2). (Thickness of TiO_2 film: 4+4 μm).

Figure 7: Diffusion coefficient (a) and life time (b) of the electron in TiO_2 *vs* the intensity of the illuminating light for device C and D.

Figure 8: Diffusion coefficient (a) and life time (b) of the electron in TiO_2 *vs* the intensity of the illuminating light for device E and F.

Table 1: The energy level of the frontier orbitals and photovoltaic performance of **SJW-B18** and CYC-B11H dyes.

Device (sensitizer)	HOMO (V *vs* NHE)	LUMO (V *vs* NHE)	*Jsc* (mAcm^{-2})	*Voc* (mV)	*FF*	η (%)	dye loading (mole)
A (SJW-B18)	0.95	-0.60	19.12	746	0.669	9.54	2.18E-8
B (CYC-B11H)	0.95	-0.61	20.18	743	0.644	9.64	2.90E-8

Thickness of TiO_2 film: 12+4 μm; Electrolyte: 0.2M LiI, 0.03M I_2, 0.6M BMII, 0.1M GuNCS, 0.5M TBP in CAN; Cell active area tested with a mask: 0.16 cm^2.

Table 2: The rate constants (or decay time) for the regeneration of the dye by I^- in electrolyte (τ_1) and electron in TiO_2 (τ_2) and the amplitude ratio of these two decay times.

Device (dye)	Decay time		Amplitude ratio
	τ_1 (μs)	τ_2 (μs)	A1 /A2
A (SJW-B18)	8.52±0.13	258.55±6.29	0.79/0.21
B (CYC-B11H)	7.92±0.11	244.02±3.61	0.77/0.23
M (N719)	5.25±0.31	283.54±5.29	0.49/0.51

Thickness of TiO_2 film: 12+4 μm; electrolyte: 0.2M LiI, 0.03M I_2, 0.6M BMII, 0.1M GuNCS, 0.5M TBP in CAN; Cell active area: 0.16 cm^2.

Table 3: The photovoltaic parameters of two sensitizers

Device	C	D	E	F
(dye)	(SJW-B18)	(CYC-B11H)	(SJW-B18)	(CYC-B11H)
Thickness of TiO$_2$	12+4 μm	12+4 μm	4+4 μm	4+4 μm
Jsc **(mA/cm^2)**	10.22	11.20	14.36	14.04
Voc **(V)**	0.720	0.703	0.829	0.784
FF	0.522	0.494	0.613	0.604
[a]**η (%) (average)**	3.84 (3.67)	3.89 (3.75)	7.30 (7.02)	6.65 (6.52)
[b]**Absorbance of the dye on TiO$_2$**	4.71E-4	6.96E-4	1.76E-4	1.87E-4
[c]**Rct (Ω)**	125	116	385	345

a: the efficiency is the average from 6 devices.

b: the absorbance of the dye on TiO$_2$ is equal to the dye loading times the absorption coefficient of the dye.

c: Rct is the charge transfer resistance between dye adsorbed TiO$_2$ and electrolyte calculated from EIS data.

Electrolyte: 0.2M Co(II), 0.02M Co(III), 0.5M TBP, 0.1M LiClO$_4$ in CAN; Cell active area tested with a mask: 0.16 cm^2.

Scheme 1:

Figure 1:

SJW-B18

CYC-B11H

Figure 2

Figure 3

LUMO

HOMO
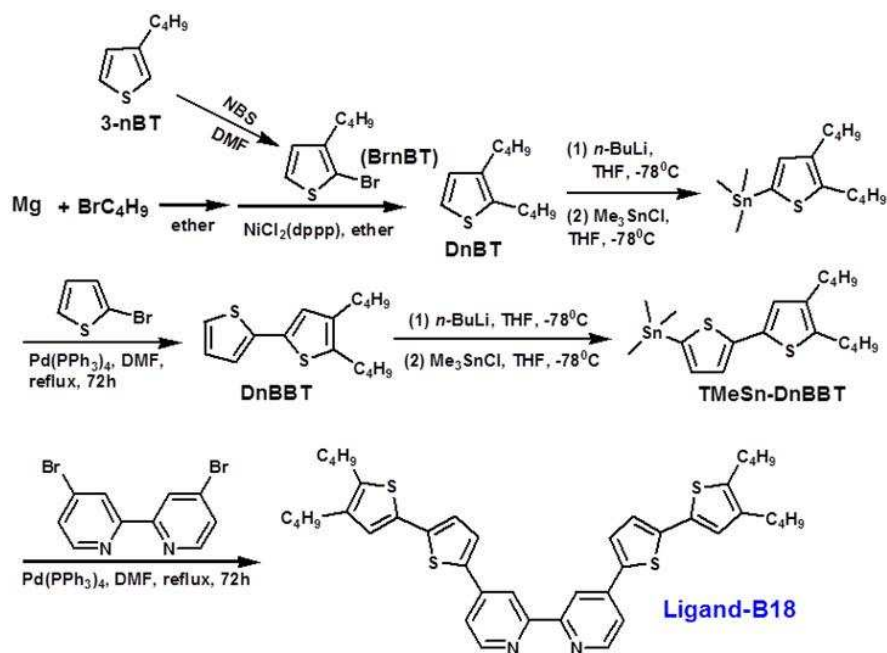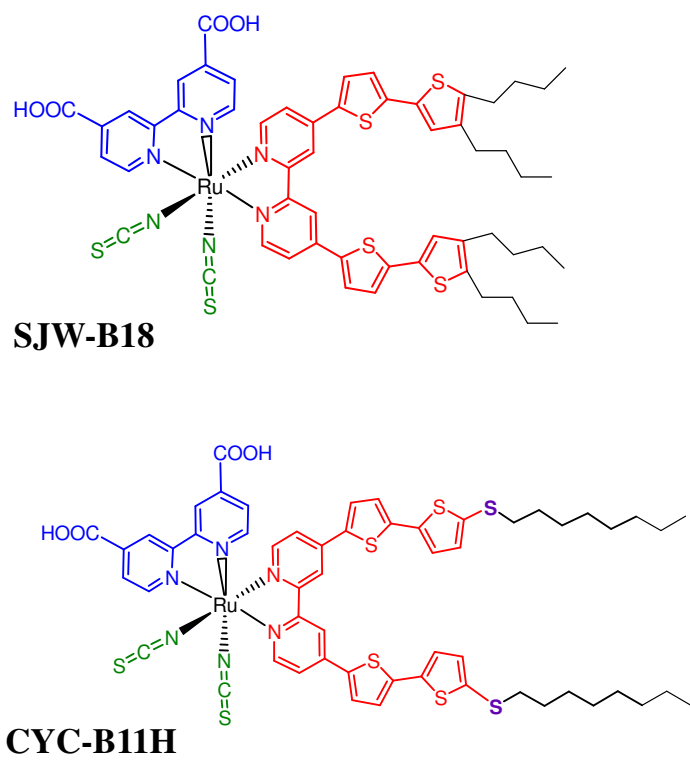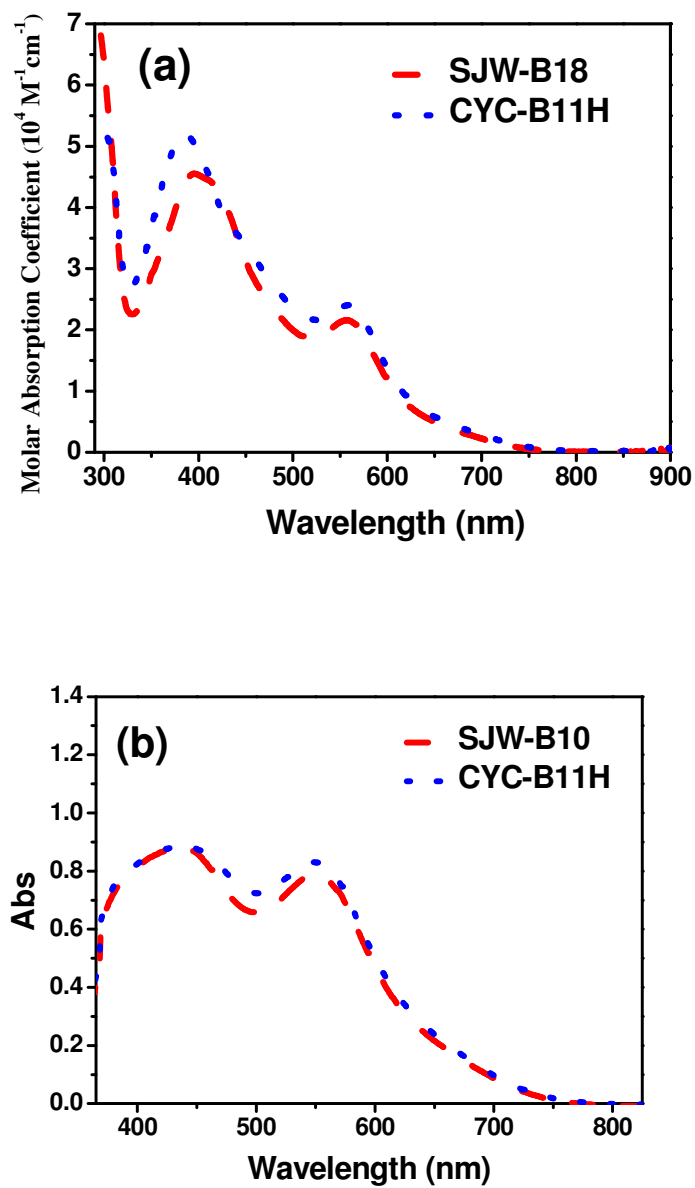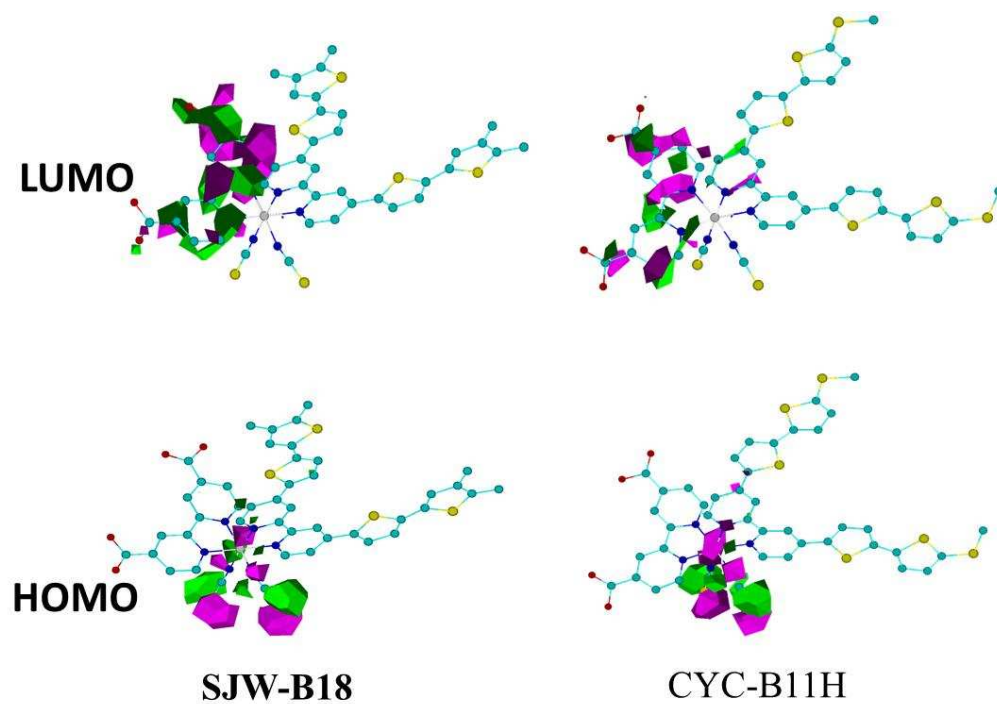
SJW-B18   CYC-B11H
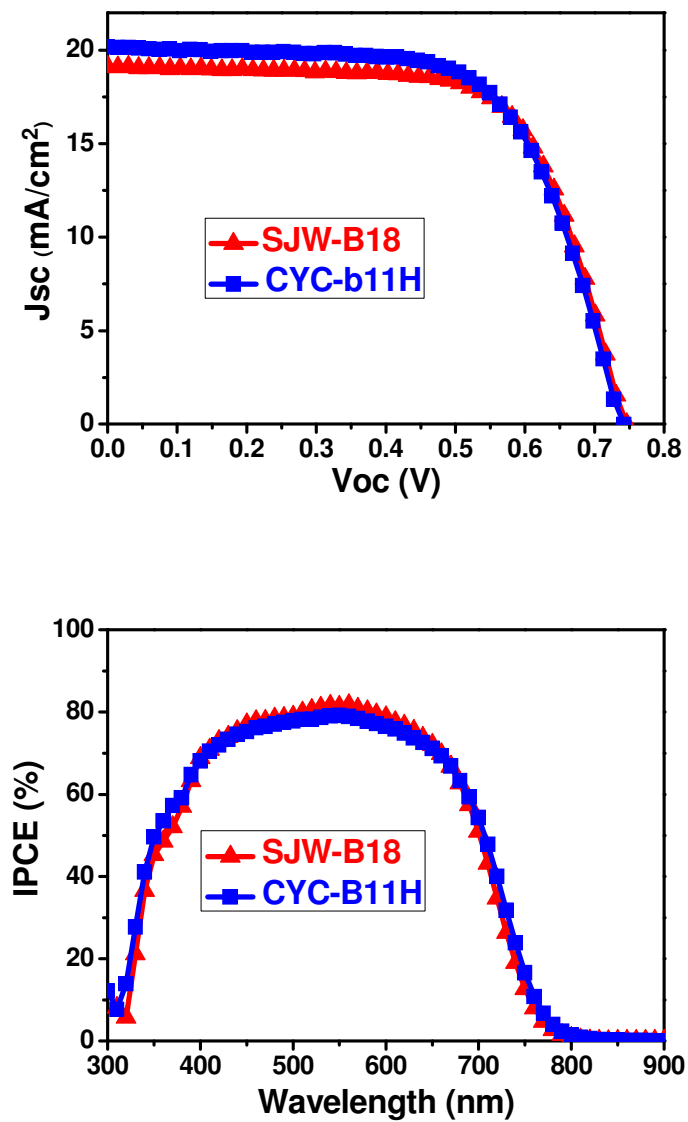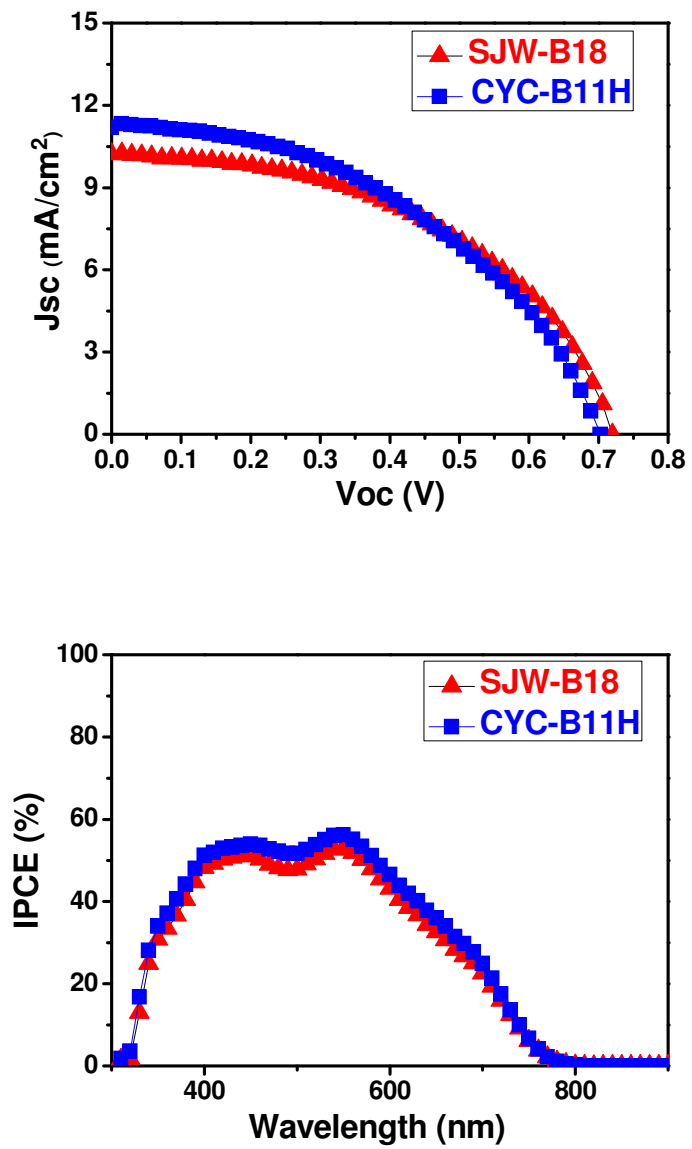
Figure 4:

Figure 5:

Figure 6:
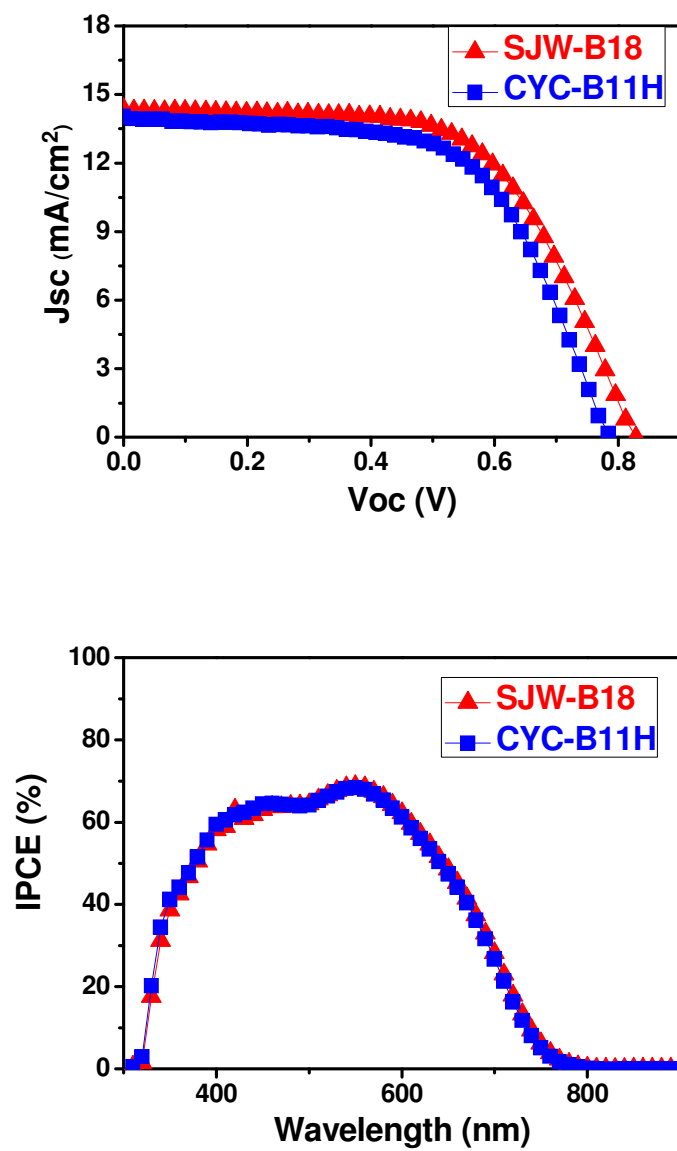
Figure 7:
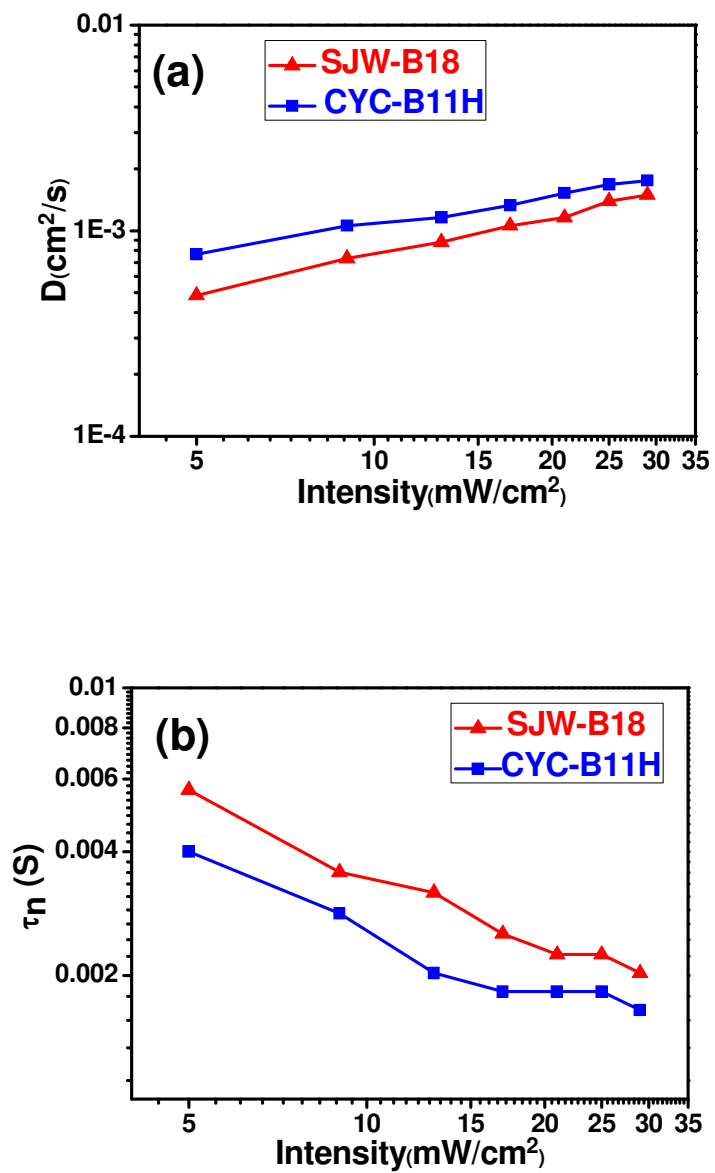
Figure 8:

_____
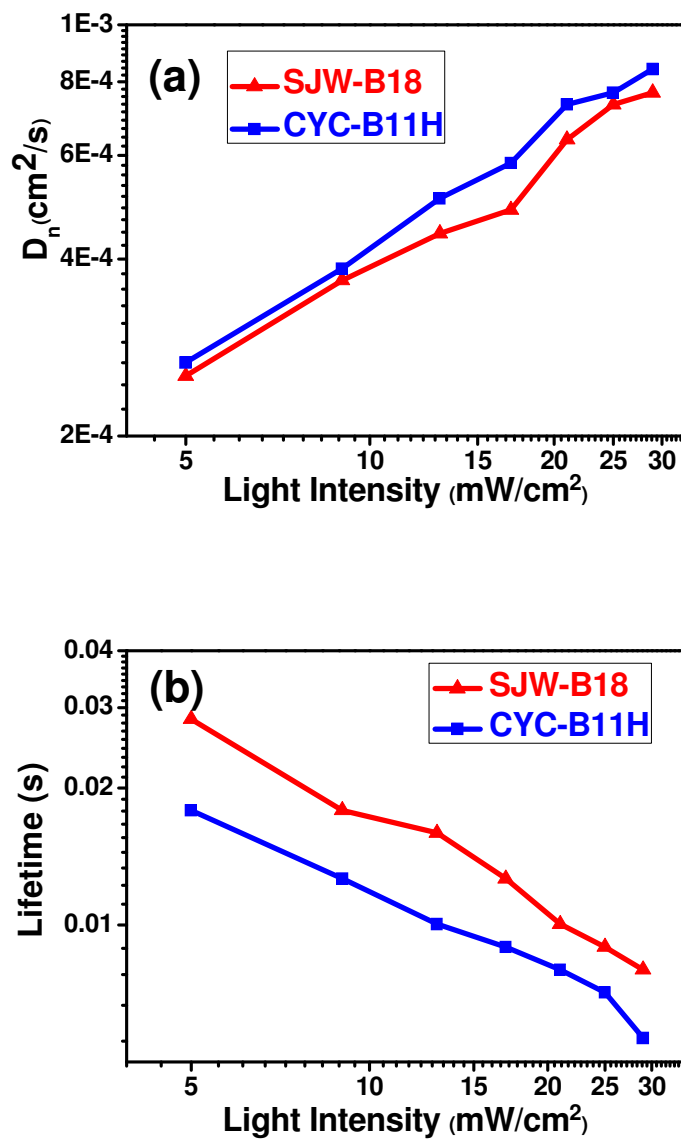
Graphical abstract
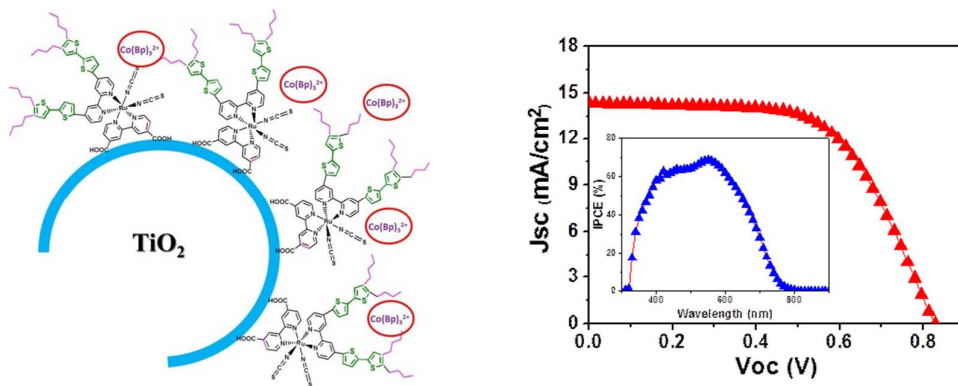
Two Ru-based dyes **SJW-B18** and CYC-B11H were prepared and their photovoltaic performance was explored. IMPS/IMVS data reveal that the physical insulation of the TiO_2 surface with four alkyl groups on **SJW-B18** can reduce the charge recombination to improve *Voc* and efficiency of the device based on cobalt electrolyte.